

A model of the ground surface temperature for micrometeorological analysis

Julian S. Leaf¹ · Evyatar Erell¹ 

Received: 7 May 2017 / Accepted: 18 June 2017 / Published online: 13 July 2017
© Springer-Verlag GmbH Austria 2017

Abstract Micrometeorological models at various scales require ground surface temperature, which may not always be measured in sufficient spatial or temporal detail. There is thus a need for a model that can calculate the surface temperature using only widely available weather data, thermal properties of the ground, and surface properties. The vegetated/permeable surface energy balance (VP-SEB) model introduced here requires no a priori knowledge of soil temperature or moisture at any depth. It combines a two-layer characterization of the soil column following the heat conservation law with a sinusoidal function to estimate deep soil temperature, and a simplified procedure for calculating moisture content. A physically based solution is used for each of the energy balance components allowing VP-SEB to be highly portable. VP-SEB was tested using field data measuring bare loess desert soil in dry weather and following rain events. Modeled hourly surface temperature correlated well with the measured data ($r^2 = 0.95$ for a whole year), with a root-mean-square error of 2.77 K. The model was used to generate input for a pedestrian thermal comfort study using the Index of Thermal Stress (ITS). The simulation shows that the thermal stress on a pedestrian standing in the sun on a fully paved surface, which may be over 500 W on a warm summer day, may be as much as 100 W lower on a grass surface exposed to the same meteorological conditions.

Keywords Storage flux · Soil moisture · Evapotranspiration · Sol-air temperature · Sub-surface ground temperature

1 Introduction – modeling surface temperature

The temperature of different urban surfaces, whether impermeable concrete, permeable bare soil or vegetation, has an effect on urban micrometeorological conditions and urban climate (Mueller and Day 2005; Yilmaz et al. 2008), on pedestrian thermal comfort (Shashua-Bar et al. 2009, 2011; Lee et al. 2016), and on energy in buildings (Meier 1990-91). Surface temperature governs two important processes: sensible heat flux and longwave radiation emitted by the surface.

Modeling schemes for urban micrometeorological conditions may incorporate any of several methods for estimating surface temperature (T_s). If most street canyon surfaces are shaded, either by buildings or vegetation, it is convenient to assign a uniform fixed surface temperature to enable the estimation of emitted longwave radiation (Krayenhoff et al. 2014). Alternatively, the temperature of shaded surfaces may be set as being equal to air temperature (T_a), while the temperature on surfaces exposed to the sun is estimated based on a linear relationship between maximum solar elevation and maximum difference between T_a and T_s during clear day conditions (Lindberg et al. 2008). The surface temperature may also be approximated by the *sol-air temperature*, $T_{\text{sol-air}}$ (Mackey and Wright 1943), which is defined as “the equivalent outdoor temperature which will cause the same rate of heat flow at the surface and the same temperature distribution throughout the material as results from the outdoor air temperature and the net radiation exchange between the surface and its environment.” In Eq. (1), T_a is the measured air temperature, K_{\downarrow} is the incoming shortwave radiation, α is the albedo of the surface, ε is its emissivity, L_{\downarrow} is the incoming

Electronic supplementary material The online version of this article (doi:10.1007/s00704-017-2207-5) contains supplementary material, which is available to authorized users.

✉ Evyatar Erell
erell@bgu.ac.il

¹ The Jacob Blaustein Institutes for Desert Research, Ben-Gurion University of the Negev, 8499000 Sde Boqer Campus, Israel

longwave radiation, L_{\uparrow} is the longwave radiation emitted from the surface, and h_c is the convective heat transfer coefficient.

$$T_{\text{sol-air}} = T_a + \frac{(1-\alpha) K_{\downarrow} - \varepsilon(L_{\downarrow} - L_{\uparrow})}{h_c} \quad (1)$$

This equation is relatively simple, and although it requires an iterative numerical solution to determine the emitted longwave radiation, it is incorporated in the Canyon Air Temperature (CAT) model (Erell and Williamson 2006). However, the sol-air temperature does not account for the thermal properties of the sub-surface material, including the thermal conductivity and heat capacity, both of which may be affected by soil moisture. It also fails to account for the effects of latent heat flux at the surface (mostly evaporation but sometimes condensation in the form of dew).

There are several methods to estimate sensible, latent, and storage heat fluxes from a moist surface—either vegetated or saturated bare soil. Penman (1948) combined an aerodynamic approach with the surface energy balance to estimate evaporation from a wet surface without knowing the surface temperature. Monteith (1965) subsequently added the effects of partially closed stomata to calculate evapotranspiration from water-stressed vegetation in what is known as the Penman–Monteith equation. Shuttleworth and Wallace (1985) further developed this equation to represent sparse crops by means of the Leaf Area Index (LAI), which enabled them to partition the effect of vegetation and the effect of bare soil while maintaining a one-dimensional representation of the fluxes.

Deardorff (1978) proposed a parameterization of surface temperature which includes a representation of a vegetation canopy layer interacting with both its underlying soil layer and the atmosphere above it. This model operates by solving energy balance equations for a bare soil surface and for a full cover vegetation canopy and by correlating the heat fluxes between these cases for a partially vegetated surface. The correlation includes fluxes of moisture and heat from both the canopy and the underlying soil to the air space within the canopy. The air space within the canopy is then used to calculate these fluxes to the atmosphere.

Best (1998) proposed a simplification of Deardorff's model of vegetation that would nonetheless result in a minimal loss of accuracy. This model assumes that the turbulent transfer between the vegetation and the soil is much smaller than the turbulent transfer into the atmosphere. By neglecting the turbulent fluxes between the vegetation and the soil for dense vegetation, the internal canopy air temperature and humidity are no longer required. The fluxes of heat and moisture into the atmosphere can then be calculated directly from the vegetation properties. This allows Best's Portable Surface Temperature (POST) model to be used in various settings with inputs that are available at a standard weather station.

Liang et al. (1994) described an energy flux model that is comprised of a two-layer characterization of the soil column and uses an aerodynamic representation of the latent and sensible heat flux at the land surface. The algorithm can account for soils with varying infiltration capacities and allows for different types of vegetation to be represented simultaneously. The actual evapotranspiration from each vegetation type is characterized by potential evapotranspiration, together with canopy resistance, aerodynamic resistance to the transfer of water, and physical resistance. The upper soil layer is defined so as to respond to rainfall events, and the lower soil layer is used to characterize the slowly varying soil moisture behavior. The ground heat flux is estimated using two thermal soil layers. The first soil layer has a varying daily temperature at the interface with the second layer which is required as an input for the model. The second (deeper) soil layer is characterized by constant soil temperature as the bottom boundary condition. The heat storage in the first soil thermal layer is assumed to be negligible. The model is formulated as a fully coupled water and energy balance system.

The Fast All-Season Soil Strength (FASST) model (Frankenstein and Koenig 2004) calculates the energy and water budget from a vegetated surface using a comprehensive multi-layer description of the soil. It quantifies both the flow of heat and moisture within the soil and also the exchange of heat and moisture at all interfaces (ground–air or ground–snow; snow–air) using both meteorological and terrain data. FASST is a very detailed model, suitable for users who have a full description of their site, and allows thermal and hydrological analysis of several terrain types including asphalt, concrete, bed rock, permanent snow, or low vegetation such as grasses, shrubs, marsh, tundra, and desert vegetation. At a minimum, the only meteorological data required is air temperature, but model performance with such limited inputs is not validated.

The objective of this research is to propose a relatively simple formulation for urban micrometeorological models that is simpler to apply than FASST or the Liang et al. method, yet which accounts for the changing thermal properties of soils in response to variations in moisture content, as well as a simplified means of describing the effect of surface cover vegetation, such as grass. The model should be capable of calculating the hourly surface temperature using only widely available data from a standard meteorological station (namely air temperature, incoming radiation, precipitation, and vapor pressure) and inputs that characterize the ground such as albedo, thermal conductivity, heat capacity, and infiltration capacity. It should require no a priori knowledge of soil temperature or moisture at any depth.

2 Methods

2.1 Model development

The vegetated/permeable surface energy balance (VP-SEB) model is based on a surface energy balance formulation combining several equations from various sources. Foremost, among these is the ground storage flux formulation proposed by Liang et al. (1994), which uses a two-layer characterization of the soil column with a prescribed boundary condition at each ground level. The sub-surface temperature is obtained using a sinusoidal function proposed by Hillel (1982), for annual and diurnal cycles. The latent heat flux is estimated using the Penman–Monteith equation (Penman 1948; Monteith 1965). A simplified procedure to describe changing soil moisture content is proposed, which then affects the latent heat flux and, in turn, the surface temperature. The energy fluxes are a function of the surface temperature itself, so an iterative procedure is used to solve the SEB equations.

The energy balance of a surface is described by the following general equation:

$$Q^* = Q_H + Q_E + \Delta Q_S \tag{2}$$

where Q^* ($W\ m^{-2}$) is the net radiative flux, Q_H ($W\ m^{-2}$) is the sensible heat flux, Q_E ($W\ m^{-2}$) is the latent heat flux, and ΔQ_S ($W\ m^{-2}$) is the change in energy stored in the soil.

2.1.1 Sensible heat flux

The sensible heat flux (Q_H) represents the energy exchange between a surface and its adjacent air and is proportional to the difference between the surface temperature (T_s , K) and the air temperature at screen height (T_a , K). This difference is multiplied by the convective heat transfer coefficient (h_c , $W\ m^{-2}\ K^{-1}$) which depends mainly on wind velocity and turbulence. The heat transfer coefficient is obtained empirically and is affected by the specific heat and density of air [C_p ($J\ kg^{-1}\ K^{-1}$) and ρ_a ($kg\ m^{-3}$), respectively] and the aerodynamic resistance (r_a , $s\ m^{-1}$) which is a function of wind speed and the stability status of the atmosphere.

The sensible heat flux is described as follows:

$$Q_H = h_c(T_s - T_a) = \frac{\rho_a C_p (T_s - T_a)}{r_a} \tag{3}$$

Rearranging Eqs. (2) and (3) gives the surface temperature

$$T_s = T_a + \frac{r_a(Q^* - Q_E - \Delta Q_S)}{\rho_a C_p} \tag{4}$$

Air temperature is obtained from the meteorological time series, but the remaining terms depend on the surface temperature as well, so an iterative scheme is used to obtain them.

There are numerous expressions relating the convective heat transfer coefficient to wind speed above the surface. As the intended application of VP-SEB is in studies of urban micrometeorological conditions, the expression proposed by Hagishima and Tanimoto (2003) was considered the most appropriate

$$h_c = 3.96\sqrt{u^2 + v^2 + w^2} + 6.42 \tag{5}$$

where u , v , and w ($m\ s^{-1}$) are the wind speed components at 0.13 m above the surface. In the case of a relatively large exposed surface, it may be possible to neglect the v and w components without compromising accuracy substantially.

Wind speed adjacent to the surface is obtained from the meteorological record using the transformation proposed by Macdonald (2000). Equation (6), which was derived from wind tunnel data, gives the relation between wind speed at two given heights, accounting for three-dimensional surface obstacles (cubes) which could be representative of a simple urban-type surface. The frontal density (λ_f), which is the ratio between the frontal area of each obstacle exposed to wind and the underlying surface area of the obstacle, governs the change of wind speed with height

$$U_{0.13} = U_{10}\exp\left(9.6\lambda_f\left(\frac{0.13}{10} - 1\right)\right) = U_{10}\exp(-9.4752\lambda_f) \tag{6}$$

2.1.2 All-wave radiation

The net radiative flux of a surface (Q^* , $W\ m^{-2}$) is the sum of the net shortwave (solar) radiation and the net longwave radiation. It can also be represented as the sum of the radiative forcing (Q' , $W\ m^{-2}$) and the emitted longwave radiation (L_\uparrow , $W\ m^{-2}$) (Eq. (7)). (Fluxes that exit the surface are considered negative and inward energy flow positive). The radiative forcing is governed by the intensity of the sun and by the temperature of the sky, as well as the albedo of the surface and its infrared absorptivity. The radiation emitted from the surface is given by the Stefan–Boltzmann law (Eq. (8)).

$$Q^* = Q' - L_\uparrow = (K_\downarrow - K_\uparrow + L_\downarrow - L_{refl}) - L_\uparrow \tag{7}$$

$$L_\uparrow = \varepsilon_s \sigma T_s^4 \tag{8}$$

$$K_\uparrow = \alpha K_\downarrow \tag{9}$$

$$L_{refl} = (1 - \varepsilon_s)L_\downarrow \tag{10}$$

where K_\downarrow ($W\ m^{-2}$) and L_\downarrow ($W\ m^{-2}$) are the incoming shortwave and longwave radiation, respectively, which are available from the meteorological time series; ε_s is the emissivity of the surface; σ ($W\ m^{-2}\ K^{-4}$) is the Stefan–Boltzmann constant (5.67×10^{-8}); L_{refl} ($W\ m^{-2}$) is the reflected longwave radiation; and K_\uparrow ($W\ m^{-2}$) is the solar radiation reflected from the

surface, depending on its albedo (α). Typical values for the surface albedo vary between 0.05 and 0.4.

The albedo of the soil (α) is also affected by moisture, with dry soils typically displaying a higher albedo. The increase in albedo with moisture is estimated by an expression following the general form proposed by Sugathan et al. (2014):

$$\alpha_{\text{dry}} = \alpha_{\text{saturated}} + C_1 \times \exp(-\theta_0/C_2) \quad (11)$$

where θ_0 is the soil moisture content and C_1 and C_2 are the empirical constants.

2.1.3 Ground storage

The ground heat flux is obtained by solving the heat diffusion equation with a prescribed boundary condition at the bottom of the solution domain. Figure 1 shows a schematic representation of the ground temperature profile, which consists of two soil layers with depths z_{mid} (m) and z_{deep} (m), respectively. At depth z_{deep} , the soil temperature variations are assumed to be negligible on a diurnal cycle, and the temperature at this depth is represented by T_{deep} (K). The temperature T_{mid} (K) at depth z_{mid} changes throughout the day.

Liang et al. (1994) described the ground heat flux by combining the representation of fluxes at each thermal soil layer. The first soil layer with depth z_{mid} is described using the thermal conductivity (λ) and the temperature at the bottom of this depth (T_{mid}), while heat storage is considered negligible

$$\Delta Q_s = \frac{\lambda}{z_{\text{mid}}} (T_s - T_{\text{mid}}) \quad (12)$$

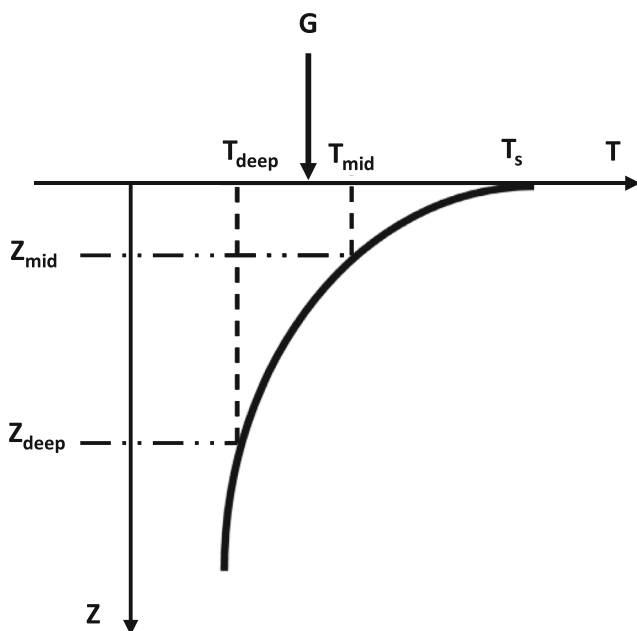


Fig. 1 Schematic representation of the sub-surface temperature profile (illustrated for the daytime). Diurnal variations decrease with depth

For the second layer with depth z_{deep} , the heat capacity (C_v) and thermal conductivity (λ) of the soil are used together with the intermediate soil temperature at the end and the beginning of a time step (T_{mid}^+ and T_{mid}^- , respectively)

$$\frac{C_v(T_{\text{mid}}^+ - T_{\text{mid}}^-)}{2\Delta t} = \frac{\Delta Q_s}{z_{\text{deep}}} - \frac{\lambda(T_{\text{mid}} - T_{\text{deep}})}{z_{\text{deep}}^2} \quad (13)$$

The volumetric heat capacity and soil thermal conductivity depend on water content (θ_0 , vol/vol), which will vary with depth. If the water table is very high, soil moisture may increase with depth. However, it is assumed here that the source of moisture is precipitation (or irrigation), so that moisture will decrease with depth and, beyond a certain depth, will remain at an equilibrium typical to the region. VP-SEB requires inputs of these properties for the dry soil and applies simplified relationships to fit experimental values reported by de Vries (1963) for different soil types.

The volumetric heat capacity is estimated as

$$C_{v_s} = C_{v_{s_{\text{dry}}}} + (4.186 \times \theta_0) \quad (14)$$

The thermal conductivity is estimated as

$$\lambda_s = \lambda_{s_{\text{dry}}} + C_3 \times \theta_0^{C_4} \quad (15)$$

where C_3 and C_4 are empirical constants.

From Eqs. (12) and (13), the ground flux is expressed as

$$\Delta Q_s = \frac{\frac{\lambda}{z_{\text{deep}}} (T_s - T_{\text{deep}}) + \frac{C_v z_{\text{deep}}}{2 \Delta t} (T_s - T_{\text{mid}})}{1 + \frac{z_{\text{mid}}}{z_{\text{deep}}} + \frac{C_v z_{\text{mid}} z_{\text{deep}}}{2 \Delta t \lambda}} \quad (16)$$

Equation (16) requires inputs for the intermediate and deep ground temperature. The VP-SEB model estimates these inputs using a sinusoidal function (Eq. (17)), following Hillel (1982). The deep ground temperature fluctuates on an annual cycle but is assumed to be constant during the course of a day. The intermediate temperature changes on a diurnal basis with intervals similar to the meteorological time series

$$T(z, t) = T_{\text{avg}} + A_0 e^{-z/d} \sin \left[\omega(t - t_0) - \frac{z}{d} \right] \quad (17)$$

Equation (17) is applied differently for an annual or a daily time scale (note the change of units)

A_0 (K) is the amplitude of the sine function $(T_{\text{max}} - T_{\text{min}})/2$, which is half of the difference between the coldest and hottest day in a year (annual use) or hour in a day (diurnal use). T_{avg} (K) is the daily or yearly averaged surface temperature. If the mean annual surface temperature is not available, the mean annual air temperature with an addition of 2° can be used (Hillel 1982).

ω (h^{-1}) or (day^{-1}) is the angular frequency ($\frac{2\pi}{P}$): $P = 365$ (days) (annual use) and $P = 24$ (h) (diurnal use).

t (h) or (days) is the unit of the time series.

t_0 (h) or (days) is the offset in hours (or days) to match the sine function to the actual measured oscillation. The yearly value is obtained for a specific geographic location by matching the sine function of daily-averaged air temperature to the results of Eq. (17). Once the value is estimated for a specific location, it can be used for shorter (or other) time periods.

d (m) is the damping depth given as $d = \sqrt{2 \frac{\lambda C}{\omega}}$.

z (m) is the desired depth.

The sinusoidal model has several characteristics: (1) the diurnal or annual temperature cycle is due to the fluctuating inputs of air temperature during a 24-h period (day/night) or during a year (summer/winter), (2) the amplitude of temperature fluctuations decreases with depth, and (3) transfer of heat down (or up) the soil levels takes time, so there is a lag in the peak temperature occurrence between different soil levels.

2.1.4 Latent heat flux

The latent heat flux is calculated using the Penman–Monteith equation

$$Q_E = \lambda_w ET = \frac{s(Q^* - \Delta Q_s) + \rho_a C_p \frac{(e_s - e_a)}{r_a}}{s + \psi \left(1 + \frac{r_s}{r_a}\right)} \quad (18)$$

where s (mb K^{-1}) is the slope of the saturation vapor pressure–temperature relationship, ψ (0.66 mb K^{-1}) is the psychrometric constant, r_s (s m^{-1}) is the surface resistance, r_a (s m^{-1}) is the aerodynamic resistance, and the product $\rho_a C_p$ is the volumetric heat capacity of the air (J m^{-3}). $e_s - e_a$ (mb) represents the vapor pressure deficit between a moist surface and the air: e_a (mb) is the vapor pressure at screen height from the meteorological time series, and e_s (mb) is the vapor pressure at the surface. Air adjacent to a wet surface is assumed to be saturated (Penman 1948; Monteith 1965).

The relationship between air temperature and saturation vapor pressure (e_s) is described by Eq. (19). The slope of the saturation vapor pressure curve (s) at a given temperature is given by Eq. (20) (Allen et al. 1998, based on Tetens 1930 and Murray 1967)

$$e_s = 6.108 \exp \left[\frac{17.27 T_a}{T_a + 237.3} \right] \quad (19)$$

$$s = \frac{4098 \left[0.6108 \exp \left(\frac{17.27 T_a}{T_a + 237.3} \right) \right]}{(T_a + 237.3)^2} \quad (20)$$

2.1.5 Surface resistance

When simulating a vegetated surface, a value in the range of 50–70 (s m^{-1}) is used for r_s of plants such as grass which are photosynthetically active during the daytime. Crassulacean acid metabolism (CAM) plants may have much higher surface resistance, with values as high as 500. Typical values for r_s are shown in Table 1.

For a bare surface, r_s depends greatly on the structure and texture of the soil. The relationship between r_s and the soil water content in the top 1–5 cm, θ_0 ($\text{m}^3 \text{ m}^{-3}$), is usually formulated with an exponential function, since surface resistance increases substantially as the soil dries out.

2.1.6 Soil moisture content

Soil moisture content can be predicted from rainfall observations using an analytical method (Pan et al. 2003) which uses a time-dependent average of cumulative rainfall over a given period, typically at least 14 days, without knowing the diffusion rate of water into the soil. The initial conditions of the soil using this method are not needed when calculating for longer periods of time.

In VP-SEB, soil moisture (θ_0) is estimated by means of a simplified balance that accounts for the effect of changes in soil moisture content through evaporation and precipitation

$$\theta_0 = \theta_0^- + \left((P^- - ET^-) \left(\frac{\gamma}{z} \right) \right) \quad (21)$$

where θ_0^- ($\text{m}^3 \text{ m}^{-3}$) is the soil moisture content from the previous time step and P^- (m s^{-1}) and ET^- (m s^{-1}) are the precipitation and evapotranspiration from the previous time step, respectively. γ is a dimensionless empirical infiltration coefficient representing the unsaturated soil’s ability to absorb any incoming water in a layer of depth z (m), with values between 0.0 for impervious surfaces such as concrete and 1.0 for loosely packed granular soils such as sand or highly porous soils such as peat. $ET^- = \frac{Q_E}{\lambda_w \rho_w}$, where λ_w (J kg^{-1}) is the latent heat

Table 1 Values of surface (or crop) resistance for different surface types (Monteith 1965; Oke 1987)

Surface	r_s (s m^{-1})	Source
Open water	0	Oke (1987)
Crops	50	
Forests	80–150	
Short grass	70	
Different types of grass		
Timothy and meadow fescue	50	Monteith (1965)
Rough pasture with some clover	50	
Ryegrass	50–110	
Alfalfa-brome mixture	40	

of vaporization of water and ρ_w (kg m^{-3}) is the density of water. Irrigation, if any, is treated as the equivalent amount of precipitation.

To account for the effect on evaporation of changes in soil moisture content, the latent heat flux obtained from the Penman–Monteith equation is multiplied by the moisture factor (M_s). For $\theta_0 > 0.25$, $M_s = 1.0$, allowing unrestricted evaporation. For $\theta_0 \leq 0.25$, $M_s = 4.0 \theta_0$, progressively restricting water loss as the soil dries. This implies a linear relationship between the moisture factor (M_s) and the soil moisture, which is clearly a simplification: as soil moisture drops below field capacity, the decline in evaporation may be expected to be exponential. However, because the thickness of the soil layer that directly affects evaporation is small— z was fixed at 5 cm—model performance was not adversely affected. Soil moisture (θ_0) is limited (arbitrarily) to a minimum value of 0.02 and a maximum value that depends on the porosity of the soil, which is about 0.4 for most soils but which may be as high as 0.8 for peat.

An estimate of the initial soil moisture content is used for a spin-up period. The sensitivity of the model to the accuracy of

this estimate declines with spin-up time, the length of which depends on the rate of evaporation and the frequency and magnitude of subsequent precipitation events. However, a spin-up period of several days may be required if the initial estimate differs substantially from the actual value of soil moisture.

2.2 Calculation procedure

1. Parameters that do not depend on surface temperature (L_{\downarrow} , K_{\downarrow} , Q' , $U_{0.13}$, h , r_a , s , e_s) are calculated using the atmospheric input parameters. These parameters will stay constant throughout the iteration (Fig. 2).
2. T_{mid} and T_{deep} are calculated for the entire desired period.
3. The energy terms ΔQ_s , Q^* , and Q_E , which also depend on the surface temperature, are calculated using the air temperature for the first iteration.
4. The surface temperature is calculated using Eq. (22), obtained by isolating the surface temperature term from Q_H

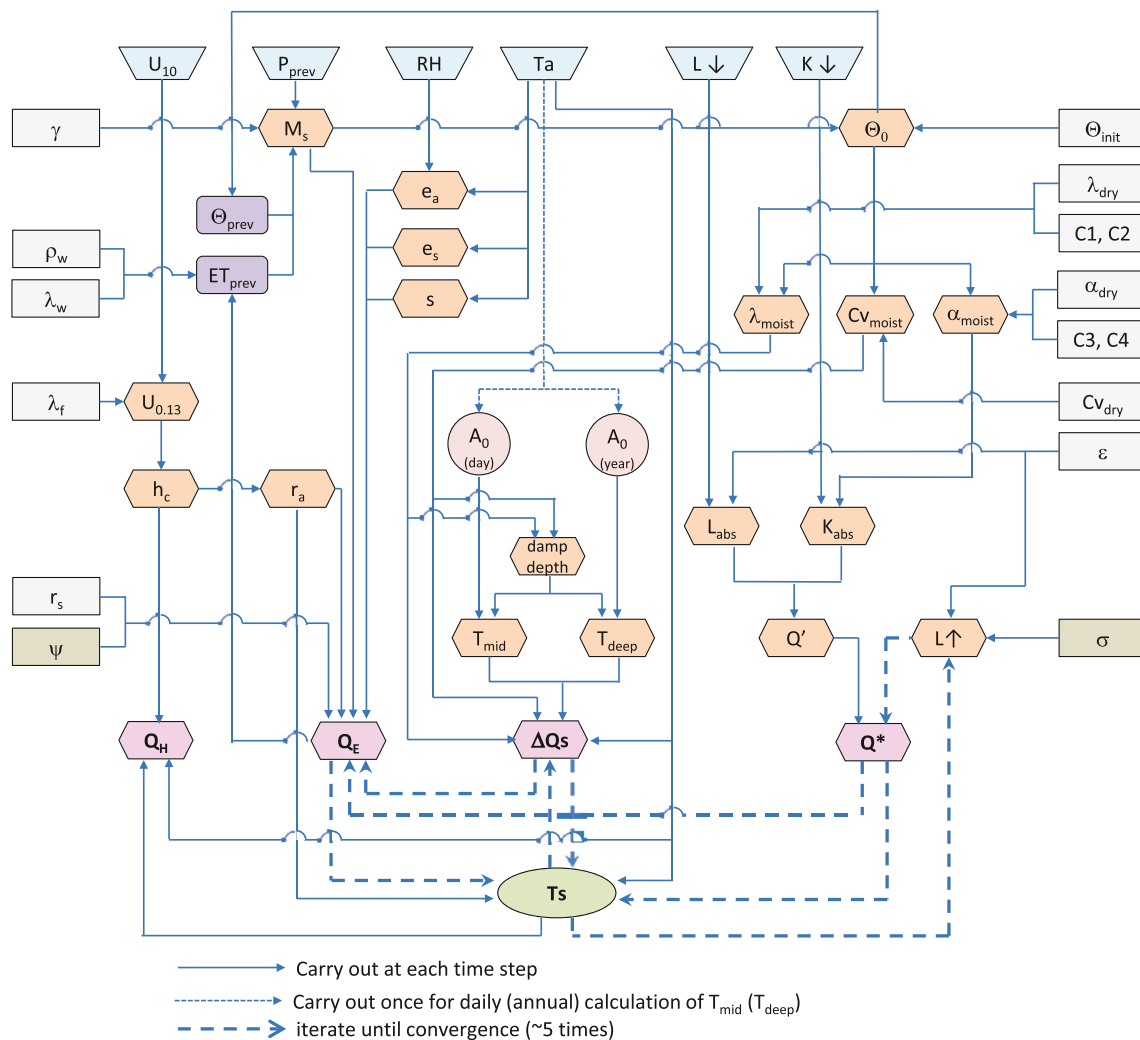


Fig. 2 Flow chart of the VP-SEB calculation procedure

and ΔQ_s in the energy balance equation following Liang et al. (1994)

$$T_s = \frac{Q^* - Q_E + \frac{\rho C_p T_a}{r_a} + \frac{\lambda}{z_{deep}} T_{deep} + \frac{C_v z_{deep}}{2 \Delta t} T_{mid}}{\frac{\rho C_p}{r_a} + \frac{\lambda}{z_{deep}} + \frac{C_v z_{deep}}{2 \Delta t}} \left(\frac{1 + \frac{z_{mid}}{z_{deep}} + \frac{C_v z_{mid} z_{deep}}{2 \Delta t \lambda}}{1 + \frac{z_{mid}}{z_{deep}} + \frac{C_v z_{mid} z_{deep}}{2 \Delta t \lambda}} \right) \quad (22)$$

5. The soil moisture content (θ_0) and M_s are updated using the calculated evapotranspiration.
6. Steps 2 to 5 are repeated using the estimated surface temperature from the previous iteration until the surface temperature converges (Fig. 2). Experience suggests that the procedure converges rapidly, and four to five iterations are sufficient.

The entire calculation is implemented in FORTRAN. The code is provided as supplementary material to this paper, as well as a sample input file.

2.3 Validation with observational data

The VP-SEB model was validated against the surface temperature of a loess soil surface under various weather conditions at the Sde Boqer meteorological station for a period of 1 year (2014) (Fig. 3). Meteorological inputs required for VP-SEB were taken from the same meteorological station (<http://bidr.bgu.ac.il/BIDR/research/phys/meteorology/default.asp>).

Sde Boqer is in the arid Negev desert of Israel at 30.8° N latitude, approximately 480 m above sea level. The climate is characterized by sharp daily and seasonal thermal fluctuations,



Fig. 3 Landscape at Sde Boqer

dry air, and clear skies with intense solar radiation. During the hot and dry summers, the mean daily maximum air temperature is approximately 33 °C, while nights dip to an average of 18 °C. Winter days are typically cool and sunny with daily mean air temperature of 14.4 °C and a nightly minimum of 3.8 °C. Prevailing winds are northwesterly and moderately strong during the late afternoon and evening (Bitan and Rubin 1994).

The soil at Sde Boqer may be characterized as a clay loam. The dry soil has a thermal conductivity of about 0.3 W m⁻¹ K⁻¹ and a volumetric heat capacity of 1.4 MJ m⁻³ K⁻¹. Soil albedo is 0.39 when dry (Snir et al. 2016) and 0.24 when wet. The organic content of the soil is negligible, and it has a very low infiltration coefficient, so that surface runoff is generated very easily following rain events of modest volume and intensity, even if the soil at a depth of several centimeters below the surface is not saturated.

Model inputs for Sde Boqer are shown in Table 2.

The model was also validated against surface temperature data for grass and asphalt, both obtained by infrared imaging (infrared thermometer, IRT) for periods of several hours on a mild spring day and a hot summer day at the Sde Boqer Campus (Snir et al. 2016).

3 Results and discussion

3.1 Statistical analysis

The quality of the modeled surface temperature was assessed by comparison of the predicted and observed values using regression analysis, error analysis, and goodness-of-fit tests.

Moriasi et al. (2007) noted that model output is compared to corresponding measured data with the assumption that all

Table 2 Inputs used for the Sde Boqer validation test

Parameter	Value
Soil albedo, saturated (dry)	0.24 (0.39)
Constants for albedo correction (C_1, C_2)	0.15, 0.15
IR emissivity of soil	0.90
Heat capacity of dry soil (MJ m ⁻³ K ⁻¹)	1.35
Thermal conductivity of dry soil (W m ⁻¹ K ⁻¹)	0.50
Constants for conductivity correction (C_3, C_4)	2.1, 0.55
Soil infiltration coefficient	0.2
Soil initial moisture content (vol vol ⁻¹)	0.15
Bulk density of dry soil (kg m ⁻³)	1600
Offset of minimum air temperature (days)	105
Soil moisture maximum (vol vol ⁻¹)	0.4
Mean annual air temperature (°C) ^a	21.4
Annual amplitude of mean daily air temperature (°C) ^a	14.6

^a These values are also calculated by the software if the weather (input) file describes an entire year

error variance is contained within the predicted values and that observed values are error free. As this is not the case in observations of earth–atmosphere interactions, they recommend that in addition to graphical techniques and standard performance measures, three quantitative statistics should be used: the Nash–Sutcliffe efficiency (NSE), percent bias (PBIAS), and the ratio of the root mean square error to the standard deviation of measured data (root-mean-square error, RSR). The Nash–Sutcliffe Efficiency Index defines the proportion of the initial variance within the observed data accounted for by the model (Nash and Sutcliffe 1970) and ranges between $-\infty$ and 1.0, with $NSE = 1$ being the optimal value. PBIAS measures the average tendency of the simulated data to be larger or smaller than their observed counterparts (Gupta et al. 1999), with an optimal value of 0.0. RSR standardizes the root-mean-square error using the observations standard deviation and has an optimal value of 0.0.

In numerous situations, the value (v) of an input variable (or a combination of several variables) can provide a fairly close approximation to the measured parameter (m). A model may only be considered useful if the estimated value of the parameter in question (e) is closer to the observed value than this trivial approximation of the input variable. According to the Williamson degree of confirmation (Williamson 1995), a model will be considered suitable if the predicted value (in this case, modeled surface temperature) will provide a better fit to the measured value than an arbitrary estimate such as the input value (in this case, measured air temperature). The indicator varies from $-\infty$ to 1.0, with values between 0.0 and 1.0 indicating an improvement relative to the arbitrary reference. This indicator is used in addition to the standard measures and the more sophisticated ones recommended by Moriasi et al. (2007), Willmott (1981, 1982), and Willmott et al. (1985).

Statistical measures of model performance are shown in Table 3.

Table 3 Statistical evaluation of the predicted surface temperature

Total number of hours	8760
Mean error	0.68
Standard deviation of error	2.68
Maximum error	10.54
Minimum error	-11.22
Root mean square error	2.77
Systematic root mean square error	0.68
Unsystematic root mean square error	2.68
Willmott index of agreement	0.99
Williamson degree of confirmation	0.73
Nash–Sutcliffe Efficiency Index	0.95
Percent bias (PBIAS)	2.72
RMSE-observed std. dev ratio (RSR)	1.03

3.2 Visualization of results and statistics

3.2.1 Annual cycle of sub-soil temperature at a depth of 30 cm

The sub-surface temperature at a depth of 30 cm, modeled by VP-SEB to estimate the ground storage flux (Eq. (17)), was compared with measured values from the Sde Boqer weather station. Figure 4 shows the evolution of this temperature over the course of a year. Modeled values show a small positive bias in summer and a small negative bias in winter, but the error is typically less than 2 K. The measured data display two instances of a rapid drop in value, in March and May, both of which are the result of substantial precipitation events. The Hillel model does not account for such phenomena, but the resultant error in the modeled surface temperature due to this discrepancy is small (see Figs. 6 and 7).

3.2.2 Regression analysis of surface temperature

The modeled surface temperature for the entire year is compared with observational data (Fig. 5), showing good agreement overall with a best-fit regression line having a slope close to unity and a negligible offset.

3.2.3 Time series for cold wet weather and hot dry weather periods

Model performance is illustrated in detail for two periods of several days each. Figure 6 shows an early spring period beginning with several dry, sunny days followed by overcast weather and a major storm that deposited 20 mm of rain over a 2-h period on March 7, providing a good test of model sensitivity to changing weather and variations in soil moisture content. Changes in soil moisture and the latent flux following

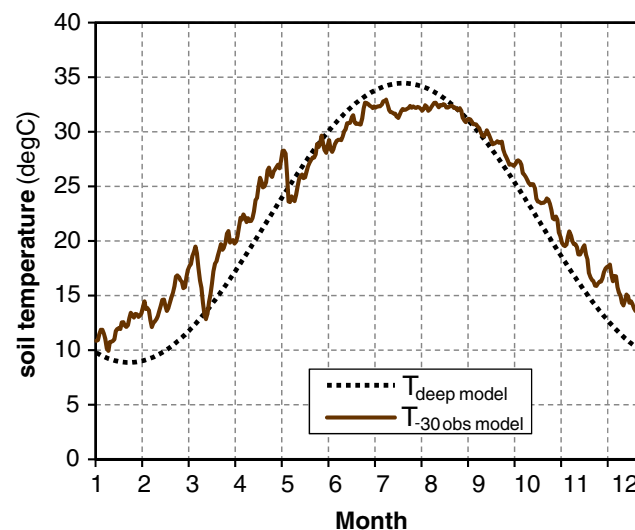


Fig. 4 Annual evolution of the mean daily sub-surface soil temperature at a depth of 30 cm

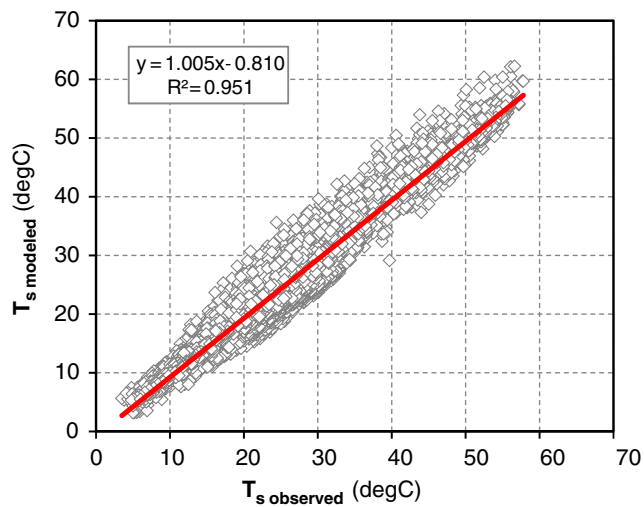
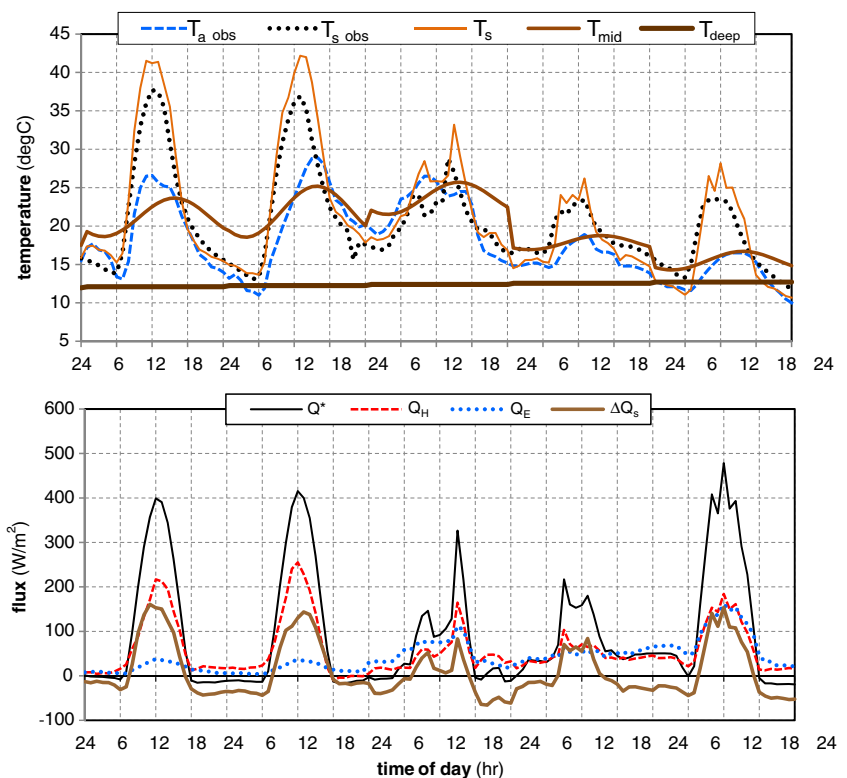


Fig. 5 X–Y plot showing hourly observed and modeled surface temperature for 2014 (8760 hourly values)

the rain are reflected in model output, as the surface temperature over the subsequent days is substantially lower than in the preceding period. The latent heat flux following the rain event remains moderate at first and increases substantially only once the daytime radiant flux is sufficient to generate substantial evapotranspiration. Figure 7 shows a hot dry summer period during which the soil is completely dry. During the daytime, modeled surface temperature is generally in good agreement with observations, while at night, there is a small negative bias. The latent heat flux during this period is extremely low.

Fig. 6 Time series showing temperature (*top*) and fluxes (*bottom*) for a 5-day period in spring (March 6–10, 2014; all values were generated by the VP-SEB model except T_{a_obs} and T_{s_obs})



3.2.4 Time series for asphalt and grass

In addition to soils, VP-SEB was designed to support modeling of the surface temperature of pavement and ground cover vegetation. In the absence of suitable long-term surface temperature data, short-term observations by an IRT were used. Although the number of data points is too small to support statistical analysis, Fig. 8 demonstrates that in principle, given appropriate inputs, the model is capable of reproducing the diurnal surface temperature pattern with acceptable accuracy. Grass surface temperature remains only a little above air temperature for most of the day (top left) and the intense sunlight offset by evapotranspiration (bottom left). Once solar radiation levels drop in the afternoon, the small grass patch is even a little cooler than the hot dry air advected from the surrounding desert. On the right, the asphalt surface temperature measures nearly 25° warmer than the air around noon (top), as most of the incoming solar radiation is absorbed in the pavement (bottom right).

3.3 Sensitivity analysis

Soil characteristics at a given location may not always be known precisely. Sensitivity analysis is used to assess the effect of inaccurate data for volumetric heat capacity, thermal conductivity, soil infiltration, and albedo on predicted surface temperature. Results of the analysis are shown in Table 4, showing the base values (in *italics>*) of the analysis (for loess

Fig. 7 Time series showing temperature (*top*) and fluxes (*bottom*) for a 5-day period in summer (July 1–5, 2014; all values were generated by the VP-SEB model except T_{a_obs} and T_{s_obs})

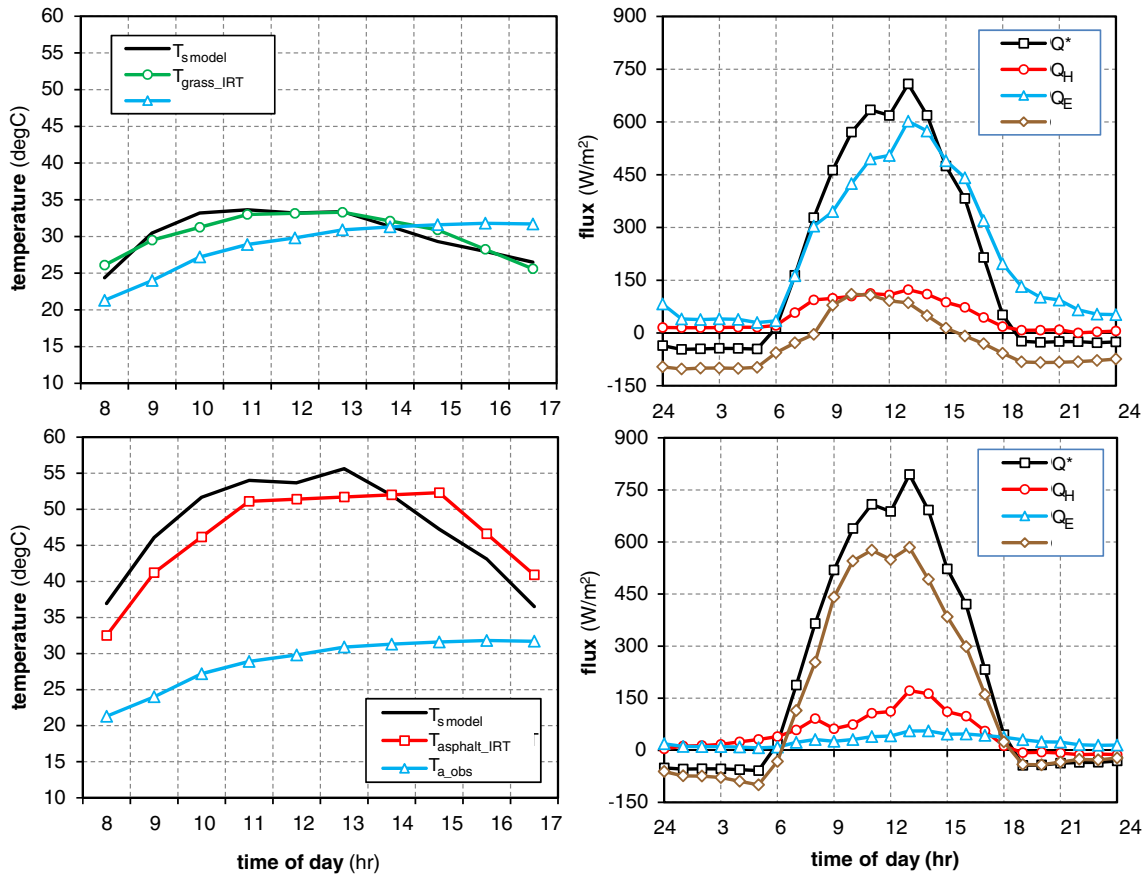
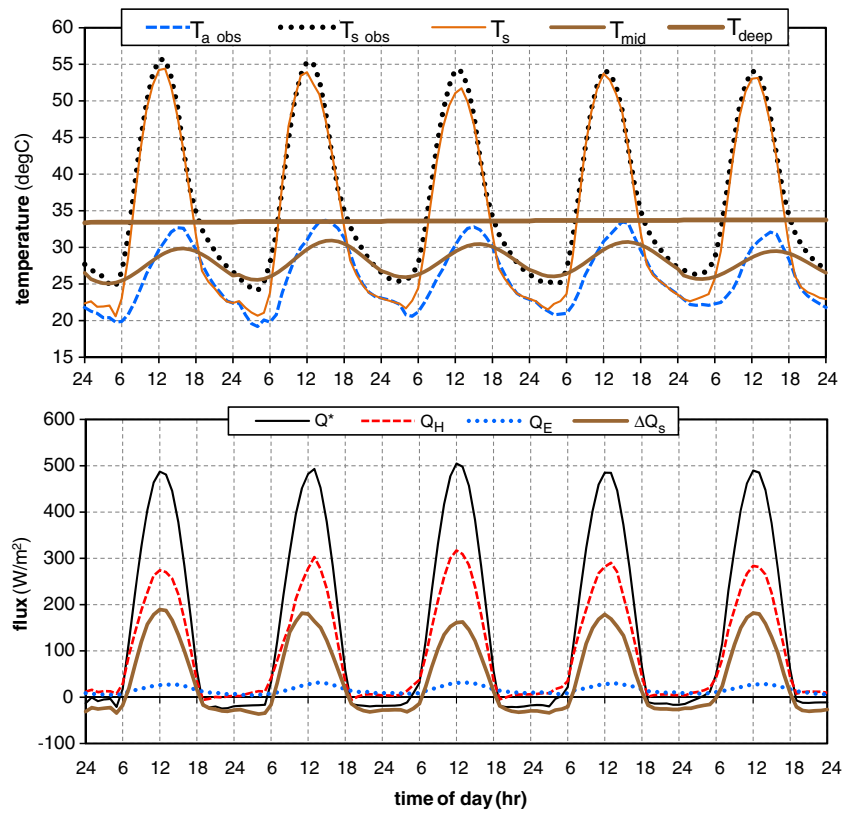


Fig. 8 Time series showing temperature (*left*) and fluxes (*right*) at Sde Boquer for a small grass plot (*top*) and for a weathered asphalt road (*bottom*). (Measured data are from Snir et al. 2016)

Table 4 Sensitivity analysis of the VP-SEB model using the Sde Boqer data

Parameter	Value	% change	Mean error	std dev	Williamson DoC	Nash–Sutcliffe
Volumetric heat capacity (mJ m ⁻³ K)	0.68	-50	0.62	2.90	0.715	0.937
	1.35	0	0.68	2.68	0.734	0.945
	2.03	+50	0.70	2.67	0.742	0.949
Thermal conductivity (W m ⁻² K)	0.25	-50	0.38	3.09	0.703	0.931
	0.50	0	0.68	2.68	0.734	0.945
	0.75	+50	0.92	2.45	0.746	0.951
Infiltration coefficient	0.10	-50	0.75	2.63	0.737	0.947
	0.20	0	0.68	2.68	0.734	0.945
	0.30	+50	0.67	2.72	0.731	0.944
Albedo (dry surface)	0.20	-50	-1.00	4.28	0.594	0.861
	0.29	-25	-0.21	3.44	0.676	0.915
	0.39	0	0.68	2.68	0.734	0.945
	0.49	+25	1.57	2.34	0.723	0.943
	0.59	+50	2.46	2.58	0.641	0.909

soil) which are used as the baseline (see also Table 1). Improved model predictions are reflected by a lower standard deviation of the error, a higher Williamson degree of confirmation, and a higher Nash–Sutcliffe Efficiency Index.

As the table shows, prediction of surface temperature is very sensitive to changes in albedo. Sensitivity to thermal conductivity and volumetric heat capacity is much lower. The sensitivity to the infiltration coefficient of the soil also appears to be low, but this may reflect the fact that Sde Boqer soil is typically dry and precipitation events infrequent.

4 Application in pedestrian thermal comfort

To simulate the effect of vegetation on pedestrian thermal stress, the VP-SEB model was run for an asphalt surface and for a vegetated surface. A negligible value of soil moisture is taken for asphalt while the grass is assumed to be well irrigated.

Thermal comfort may be described by the Index of Thermal Stress (ITS), which expresses the overall energy exchange between a human body and its surrounding environment. The ITS is adjusted for urban surroundings and expresses the latent heat of sweat evaporation that is required for a human body to maintain a thermal equilibrium with the environment (Givoni 1963; Pearlmutter et al. 2007)

$$ITS = \frac{R_n + C + (M-W)}{f} \tag{23}$$

$$R_n = (K_{dir} + K_{dif} + \alpha_h K_h + \alpha_v K_v)(1-\alpha_s) + L_d + L_h + L_v - \epsilon_s \sigma T_s^4 \tag{24}$$

where R_n is the net radiation for a body, C is the heat convection from a body, $M-W$ is the net internal body heat production accounting for metabolism (M) and work (W), and f is the efficiency of sweat evaporation. K is the shortwave solar radiation (direct and diffuse); αK is the reflected shortwave radiation (from horizontal and vertical surfaces); α_s is the body surface albedo; L is the longwave radiation emitted from the surfaces (downwards, horizontally, and vertically). ϵ_s and T are the surface emissivity and temperature of the body. The energy value of ITS (watts) is correlated with a subjective thermal sensation scale based on surveys: *comfortable* (ITS < 160), *warm* (160 < ITS < 480), *hot* (480 < ITS < 800), and *very hot* (ITS > 800).

The inputs for the ITS model include the location and time of day (required to calculate the sun position), building heights and street width, hourly meteorological data, and surface temperature. A time series of the ITS was generated in order to evaluate the effect of replacing an asphalt surface with a vegetated surface.

Figure 9 shows the effect on pedestrian thermal stress of replacing asphalt pavement with grass in a hypothetical open space in hot, dry weather, as estimated by the ITS using the ground surface temperature shown in Fig. 8. As the figure shows, the combination of relatively high air temperature, moderate humidity, low wind speed, and intense sunlight results in hot conditions for an exposed pedestrian. However, a full plant cover was found to reduce the thermal stress on a pedestrian by as much as 100 W compared to a fully paved surface. These results agree with ITS values calculated from surface temperature measurements reported by Snir et al. (2016).

The reduction in thermal stress due to the planted surface in these meteorological conditions is equivalent to the effect of lowering the dry bulb air temperature by approximately 8 °C, all else being unchanged.

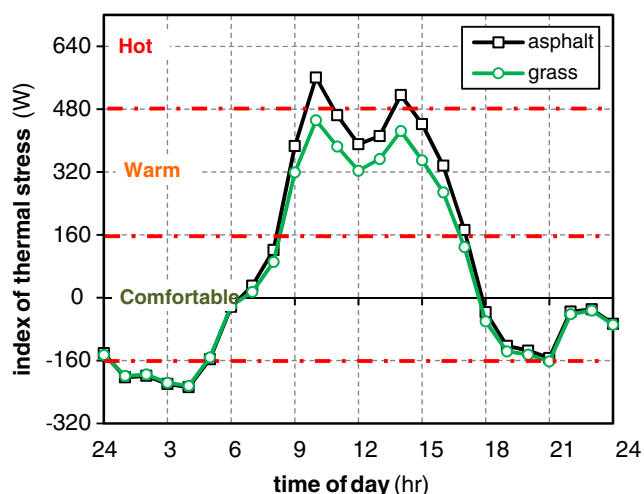


Fig. 9 The effect on pedestrian thermal stress of replacing asphalt with grass (ITS values of -160 – 160 W are considered “comfortable,” 160 – 480 “warm,” 480 – 800 “hot,” and above 800 “very hot”)

5 Discussion

VP-SEB is formulated to calculate surface temperature on small uniform patches of the urban surface and to support estimates of thermal comfort or building energy consumption at the scale of meters to tens of meters. Consequently, it does not incorporate spatial averaging of non-uniform surfaces. This is justified because horizontal fluxes of heat in the soil are negligible at this scale. In the case of a non-uniform environment, such surfaces must be resolved independently. Their overall effect may then be calculated using view factors and area-weighting schemes, as appropriate to the objectives of the procedure.

Solution of the surface energy balance requires wind speed near the surface. The heterogeneity of the urban area results in substantial variations in this datum in space and time, which are difficult to resolve even with the most sophisticated models. VP-SEB employs a simplified relationship (Eq. (6)) that does not account for the roughness of individual facets of the urban canyon and the presence of street furniture, trees, or automobiles. It also fails to account for variations in the shape of the velocity profile due to atmospheric stability conditions. However, such compromises were deemed acceptable in the absence of any practical alternative.

In most urban micrometeorological studies, the storage flux (ΔQ_s) is obtained as a residual once the other fluxes have been determined. This approach necessarily leads to closure of the surface energy balance: all errors in estimation of the other fluxes are reflected in this value. However, as Masson et al. (2002) noted, “closure of measured energy balances is rarely achieved over simple sites where micrometeorological theory is most likely to hold.” VP-SEB estimates ΔQ_s directly from the difference between the deep soil temperature (obtained by means of the Hillel prognostic model) and the surface

temperature, which is obtained from the iterative numerical process that satisfies the surface energy balance. However, this does not eliminate all possible errors, because of the simplified parametric procedures employed in VP-SEB. Therefore, although the overall error in the surface temperature is relatively small, there may still be discrepancies in some of the fluxes such that closure does not necessarily occur at all times.

Unlike most urban micrometeorological models, which are forced by atmospheric properties of the urban boundary layer, the forcing data required to run VP-SEB are obtained from a weather station in the vicinity, which measures near-surface conditions. This has the advantage of much better availability of the data, at the potential expense of errors introduced by intra-urban variability. This means that VP-SEB is best suited for integration in models of the urban street canyon, such as CAT, for which it was developed, or models such as the urban climate generator scheme proposed by Bueno et al. (2013), but not TEB (Masson 2000).

The application of VP-SEB is presently limited by the following restrictions:

- Because modeling the ground storage flux requires an estimate of the soil temperature at a depth of 30 cm below the surface, based on the Hillel model, it cannot be applied where the sine form of this model does not apply—such as near the equator. This restriction may be relaxed in practice, if the sub-surface soil temperature in such regions is almost constant, by setting the annual amplitude of the temperature equal to zero, but this approach was not tested here.
- VP-SEB cannot model snow or frozen soils.
- VP-SEB employs a very rudimentary scheme to estimate soil moisture and assumes that all soil moisture originates locally, from precipitation or irrigation. Surface or sub-surface flows of water are not modeled. Also not accounted for is moisture that may originate in a high water table.
- Water loss by evapotranspiration is controlled only by the effect of solar radiation and wind and is not restricted by the changing hydraulic resistance of the soil as it dries. Water content at saturation is limited by pore space (about 40% for most soils) and is allowed to drop down to a minimum of 2%.
- The coupling of the surface cover vegetation to the underlying soil substrate is assumed to occur by conduction only, via plant roots or direct contact of the foliage. VP-SEB does not model an intermediate air layer and is thus suited for modeling grass or ground-cover succulents but not bushes.

Validation of the VP-SEB model for an extended period was carried out using data from only one location. Although

the goodness-of-fit tests for this location were satisfactory, the model will certainly benefit from evaluation using other data sets. In particular, a long-term record of the surface temperature of vegetation, such as grass, will improve confidence in the model's robustness for such surfaces.

6 Conclusions

The objective of this research was to develop a relatively simple model for the surface temperature of a permeable or vegetated surface using a physically based solution for the energy fluxes. The VP-SEB model requires only widely available data from a standard meteorological station and inputs that describe the surface—albedo, thermal conductivity, heat capacity, and infiltration capacity. It requires no a priori knowledge of soil temperature or moisture at any depth, nor does it require any other descriptors of the atmosphere. Rather, the surface temperature was modeled using an iterative procedure that combines a two-layer representation of the soil column with a sinusoidal function for calculating the ground flux, and a simplified procedure to describe changes in moisture content with a minimal loss of accuracy.

Statistical analysis showed that VP-SEB's modeled surface temperature is a close proxy of the measured data and is therefore suitable for analysis and integration in local-scale micrometeorological models. Application of the model was demonstrated in a simple scenario assessing the thermal stress on a pedestrian standing on either aged asphalt or grass. Although the albedo of both surfaces is low, the model indicates a substantial difference in surface temperature, which is then reflected in the Index of Thermal Stress.

Surface properties such as radiant temperature and albedo play an important role in determining the total thermal stress on a person. It is hardly new that the use of vegetation as a surface cover can reduce such stress in over-heated conditions. However, many of the prior studies on the effects of urban green are empirical and describe only one site and a limited range of vegetation. This study provides the basis for a method for quantifying these effects in a variety of environmental conditions, especially during elevated heat stress.

Acknowledgements This research was made possible with the support of the Jewish National Fund.

References

- Allen R, Pereira L, Raes D, Smith M (1998) Crop evapotranspiration—guidelines for computing crop water requirements—FAO irrigation and drainage paper 56. FAO 56.
- Best M (1998) A model to predict surface temperatures. *Bound-Layer Meteorol* 88:279–306
- Bitan A, Rubin S (1994) Climatic atlas of Israel for physical and environmental planning and design. Ramot Publishing Company, Tel-Aviv University, Tel-Aviv
- Bueno B, Norford L, Hidalgo J, Pigeon G (2013) The urban weather generator. *J Build Perform Simul* 6:269–281
- De Vries D (1963) Thermal properties of soils. In: van Wijk W (ed) *Physics of plant environment*. North-Holland Publishing Company, Amsterdam, pp 210–235
- Deardorff JW (1978) Efficient prediction of ground surface temperature and moisture, with inclusion of a layer of vegetation. *J Geophys Res Oceans* 83:1889–1903
- Erell E, Williamson T (2006) Simulating air temperature in an urban street canyon in all weather conditions using measured data from a reference meteorological station. *Int J Climatol* 26:1671–1694
- Frankenstein S., Koenig G. 2004. FASST vegetation models. ERDC/CRREL TR-04-25.
- Givoni B (1963) Estimation of the effect of climate on man—development of a new thermal index. Technion-Israel Institute of Technology, PhD thesis, Haifa
- Gupta H, Sorooshian S, Yapo P (1999) Status of automatic calibration for hydrologic models: comparison with multilevel expert calibration. *J Hydrol Eng* 4:135–143
- Hagishima A, Tanimoto J (2003) Field measurements for estimating the convective heat transfer coefficient at building surfaces. *Build Environ* 38:873–881
- Hillel D (1982) *Introduction to soil physics*. Academic, San Diego
- Krayenhoff ES, Christen A, Martilli A, Oke TR (2014) A multi-layer radiation model for urban neighbourhoods with trees. *Bound-Layer Meteorol* 151:139–178
- Lee H, Mayer H, Chen L (2016) Contribution of trees and grasslands to the mitigation of human heat stress in a residential district of Freiburg, Southwest Germany. *Landsc Urban Plan* 148:37–50
- Liang X, Lettenmaier DP, Wood EF, Burges SJ (1994) A simple hydrologically based model of land surface water and energy fluxes for general circulation models. *J Geophys Res-Atmos* 99:14415–14428
- Lindberg F, Holmer B, Thorsson S (2008) SOLWEIG 1.0—modelling spatial variations of 3D radiant fluxes and mean radiant temperature in complex urban settings. *Int J Biometeorol* 52:697–713
- Macdonald RW (2000) Modelling the mean velocity profile in the urban canopy layer. *Bound-Layer Meteorol* 97:25–45
- Mackey CO, Wright LT (1943) Summer comfort factors as influenced by the thermal properties of building materials. *Transactions of the American Society of Heating and Ventilating Engineers* 49:148
- Masson V, Grimmond CSB, Oke T (2002) Evaluation of the town energy balance (TEB) scheme with direct measurements from dry districts in two cities. *J Appl Meteorol* 41:1011–1026
- Masson V (2000) A physically-based scheme for the urban energy budget in atmospheric models. *Bound-Layer Meteorol* 94:357–397
- Meier AK (1990–91) Strategic landscaping and air-conditioning savings: a literature review. *Energy and Buildings* 15-16:479–486
- Monteith JL (1965) Evaporation and environment. *Symp Soc Exp Biol* 90:205–234
- Moriasi DN, Arnold JG, Van Liew MW, Bingner RL, Harmel RD, Veith TL (2007) Model evaluation guidelines for systematic quantification of accuracy in watershed simulations. *Trans Am Soc of Agric Biological Eng* 50:885–900
- Mueller E, Day T (2005) The effect of urban ground cover on microclimate, growth and leaf gas exchange of oleander in Phoenix, Arizona. *Int J Biometeorol* 49:244–255
- Murray FW (1967) On the computation of saturation vapor pressure. *J Appl Meteorol* 6:203–204
- Nash J, Sutcliffe J (1970) River flow forecasting through conceptual models part I—a discussion of principles. *J Hydrol* 10:282–290
- Oke TR (1987) *Boundary layer climates*. Methuen, London

- Pan F, Peters-Lidard C, Sale M (2003) An analytical method for predicting surface soil moisture from rainfall observations. *Water Resour Res* 39(11):1314. doi:10.1029/2003WR002142
- Pearlmutter D, Berliner P, Shaviv E (2007) Integrated modeling of pedestrian energy exchange and thermal comfort in urban street canyons. *Build Environ* 42:2396–2409
- Penman HL (1948) Natural evaporation from open water, bare soil and grass. *Proceedings of the Royal Society of London, Series A Mathematical and Physical Sciences* 193:120–145
- Shashua-Bar L, Pearlmutter D, Erell E (2009) The cooling efficiency of urban landscape strategies in a hot dry climate. *Landsc Urban Plan* 92:179–186
- Shashua-Bar L, Pearlmutter D, Erell E (2011) The influence of trees and grass on outdoor thermal comfort in a hot-arid environment. *Int J Climatol* 31:1498–1506
- Shuttleworth WJ, Wallace JS (1985) Evaporation from sparse crops—an energy combination theory. *Q J R Meteorol Soc* 111:839–855
- Snir K, Pearlmutter D, Erell E (2016) The moderating effect of water-efficient ground cover vegetation on pedestrian thermal stress. *Landsc Urban Plan* 156:1–12
- Sugathan N, Biju V, Renuka G (2014) Influence of soil moisture content on surface albedo and soil thermal parameters at a tropical station. *J Earth Syst Sci* 123:1115–1128
- Tetens O (1930) Über einige meteorologische Begriffe. *z. Geophys* 6: 297–309
- Williamson TJ (1995) A confirmation technique for thermal performance simulation models. *Building Simulation '95*, August 14–16, 1995, Madison, Wisconsin, U.S.A
- Willmott C (1982) Some comments on the evaluation of model performance. *Bull Am Meteorol Soc* 63:1309–1313
- Willmott C, Ackleson S, Davis R, Feddema J, Klink K, Legates D, O'Donnell J, Rowe C (1985) Statistics for the evaluation and comparison of models. *J Geophys Res* 90:8995–9005
- Willmott CJ (1981) On the validation of models. *Phys Geogr* 2: 184–194
- Yilmaz H, Toy S, Irmak M, Yilmaz S, Bulut Y (2008) Determination of temperature differences between asphalt concrete, soil and grass surfaces of the city of Erzurum, Turkey. *Atmosfera* 21: 135–146